IEEE Robotics and Automation Letters (RA-L) paper, presented at ICRA 2024, Yokohama, Japan. Cite as RA-L paper.

External Dynamics Dependent Human Gait Adaptation using a Cable-Driven Exoskeleton

Sanjeevi Nakka and Vineet Vashista*, Member, IEEE

***Abstract*—The emergence of exoskeleton technology has enabled new opportunities for gait rehabilitation, but effective methods to restore healthy gait patterns with exoskeletons are not yet clearly understood. Early research in robot-based gait rehabilitation offered little improvement over current standards of physical care and emphasized the need for a deeper understanding of the complex interaction between humans and the robot, i.e., physical human-robot interaction (pHRI). Studies reported varied lower limb responses for a similar intervention with different exoskeletons, implying that the exoskeleton's external dynamics affect musculoskeletal adaptation outcomes. Accordingly, the current study aims at showcasing the external dynamics dependent gait adaptation using a Cable-Driven Leg Exoskeleton (CDLE). A swing phase gait intervention using three different CDLE cable-routing configurations that impose varied dynamics at human anatomical joints is studied. Twenty-four healthy participants, eight for each CDLE configuration, were tested. Results showed varied gait adaptation among the three groups such that the subjects used either predominantly their hip joint, knee joint, or a combination of both joints implying selective joint strategy adaptations for different external dynamics conditions for the same intervention. The results of this study can provide insights into the optimal design of leg exoskeleton-based rehabilitation paradigms for effective gait rehabilitation.**

I. Introduction

Neurological disorders and aging compromise human mobility and induce impaired gait patterns, which manifest as abnormal gait kinematics. Asymmetric interleg kinematics, reduced stride length, and reduced walking speeds are some commonly observed gait abnormalities in patients with neurological disorders [1]–[3]. Because impaired and restricted mobility negatively affects health and quality of life, developing interventions to recover or maintain healthy gait patterns is desirable.

Advances in exoskeleton technology enabled new opportunities for gait rehabilitation [4]–[6]. The emergence of lab-based and portable robotic exoskeletons facilitated the delivery of the desired gait interventions both in the lab and outdoor walking environments.However, effective methods to restore healthy gait patterns with exoskeletons are not yet clearly understood [7]–[10].

Restoration of healthy gait patterns is non-trivial. Early research in robot-based gait rehabilitation offered little improvement over current standards of physical care [7], [8]. This was likely due to the use of pre-programmed kinematics and high-gain trajectory-tracking [11], which may have discouraged the active engagement of patients in making movements and/or suppressed the natural dynamics of walking [12], [13]. Most previous designs for assistive and rehabilitation robots are functional in delivering the required outputs and performing desired tasks. Still, their effectiveness is questioned due to insufficient knowledge about the perceived interaction between humans and robots, i.e., physical human-robot interaction (pHRI) [7]. This led to the evolution of a human-centric approach to design. Consequently, to improve pHRI, several major aspects are considered, such as anthropomorphic design, alignment of joints, body fixations, quick donning and doffing, and actuation control [7]–[9].

Studies reported adaptations in the human walking pattern when external forces are applied using exoskeletons, implying some adjustments by the human musculoskeletal system [4], [7]–[9]. Studies have also reported varied adaptation outcomes when comparable interventions are applied [14]–[16]. In particular, these studies aim to alter a participant's step height during walking using exoskeletons with different structural and control designs and mobility constraints. Thus, the adopted protocol, imposed dynamics, and the control approach are essential to a leg exoskeleton-based intervention paradigm.

The current work focuses on studying the effect of the imposed dynamics on the intervention outcome. To achieve this, a gait intervention was applied using an exoskeleton with varied dynamics while maintaining a similar experimental protocol and control. We developed a treadmill-based Cable-Driven Leg Exoskeleton (CDLE) to achieve this. Due to the cables' unidirectional force application property, the CDLE has redundantly actuated cables [18]. This facilitates the implementation of the desired joint torque intervention even when the system parameters, namely, the cable-routing architecture and attachment locations, are varied. Thereby enabling the imposition of diverse external dynamics on the wearer's anatomical joints.

A swing phase force intervention to increase the step height during walking was implemented with three different imposed dynamics conditions by CDLE in this work. Twenty-four healthy participants were recruited for the study, eight for each imposed dynamics condition. The objective is to study

* Corresponding Author

Manuscript received: 15 March 2023; Revised 20 June 2023; Accepted 14 July 2023. This paper was recommended for publication by Editor Aniket Bera upon evaluation of the Associate Editor and Reviewers' comments. [Note that the Editor is the Senior Editor who communicated the decision; this is not necessarily the same as the Editor-in-Chief.]

This work involved human subjects in its research. Approval of all ethical and experimental procedures and protocols was granted by Indian Institute of Technology Gandhinagar Ethics Committee, under Application No. IEC/VV/2021/013

The authors are with the Human-Centered Robotics Lab, IIT Gandhinagar, Gandhinagar, Gujarat 382055, India (e-mail: nakka.suryasatyasanjeevi@iitgn.ac.in; vineet.vashista@iitgn.ac.in).

Digital Object Identifier (DOI): see top of this page.

IEEE Robotics and Automation Letters (RA-L) paper, presented at ICRA 2024, Yokohama, Japan. Cite as RA-L paper.

IEEE Robotics and Automation Letters (RA-L) paper, presented at ICRA 2024, Yokohama, Japan. Cite as RA-L paper.

if altering imposed dynamics conditions for a similar gait intervention affects the adaptation outcome. To check if such imposition of distinct external dynamics at anatomical joints promotes a particular joint, distal or proximal, strategy in lower-limb during walking.

II. Materials and Methods

A. CDLE Design

A Cable-Driven Leg Exoskeleton (CDLE) is developed for implementing the force intervention during treadmill walking as part of this work. Cables in a cable-driven system can be connected to the lower limb thigh and shank segments, anterior and posterior, to apply a pulling force on a segment that may either assist or resist the limb movement. The use of cables makes the CDLE lightweight and flexible, which does not restrict natural limb motion. In the current study, CDLE with four actuated cables is considered, Fig. 1(a). The modular design of the system offers flexibility in changing the positions of the actuators, pulleys, and cable anchor points to achieve varied cable routing architectures as shown in Fig. 3 (cable routing choices are presented in Section III). The components of the CDLE that are to be donned by the participants are divided into the Pelvis unit, Thigh unit, Shank unit, and Inertial Measurement Unit (IMU), as shown in the Fig. 1(a).

The pelvis, thigh, and shank units comprise a flexible brace made of polypropylene and are equipped with flexible Velcro straps and anchor points to attach the cables. The anchor points are facilitated by T-shaped components made of Delrin. The cable is mounted on one end of the T shape, and the longer portion is attached to the brace to distribute the force over the unit. Further, additional 3D-printed components and pulleys are affixed to the braces to facilitate the alteration of the cable routing architecture. These units also have attachments to mount the hip and knee joint encoder modules. The IMU unit has a flexible velcro strap and is mounted on the lower end of the shank (just above the ankle), as shown in Fig. 1(a). This unit is used for detecting the heel strike and toe-off events during walking and for computing the gait phase.

Four Brush-less DC motors (BLDC) (Model: 412821) with gearbox (Model: 412821; reduction 12:1), and motor drivers (EPOS 4 Compact 50/8 CANOpen) from Maxon (Sachseln, Switzerland) are used to actuate four cables of the CDLE. These motors are mounted on the Aluminium (Al) extrusion frame. A cable reel of 50 mm diameter is connected to the gearbox shaft through a rigid coupling. Further, Aluminium pulleys are mounted on the extrusion frame to facilitate the desired cable routing as shown in Fig. 1(a).

B. CDLE System Modelling

A cable is a unidirectional force application element, i.e., it applies only a pulling force on a body. Thus, a cable-driven system requires redundant actuation, i.e., at least *m* = (*n* + *1*) cables are required to control a *n* degrees of freedom (DOFs) system [18]. Typically, cables in a cable-driven system are modeled as a pure force at the attachment point to evaluate the applied torque, τ, at the desired joint using Lagrange's method [18].

$$\tau = \mathbf{A}T \tag{1}$$

$$\underbrace{\begin{bmatrix}\tau_{hip}\\ \tau_{knee}\end{bmatrix}}_{\tau} = \underbrace{\begin{bmatrix}\hat{l}_1.\frac{\partial \vec{r}_1}{\partial \theta_h} & A_{12} & A_{13} & \hat{l}_4.\frac{\partial r_4}{\partial \theta_h}\\ \hat{l}_1.\frac{\partial \vec{r}_1}{\partial \theta_k} & \hat{l}_{22}.\frac{\partial \vec{r}_2}{\partial \theta_k} & \hat{l}_{32}.\frac{\partial \vec{r}_{32}}{\partial \theta_k} & \hat{l}_4.\frac{\partial \vec{r}_4}{\partial \theta_k}\end{bmatrix}}_{\mathbf{A}} \underbrace{\begin{bmatrix}T_1\\ T_2\\ T_3\\ T_4\end{bmatrix}}_{T} \tag{2}$$

$$A_{12} = \hat{l}_{22}.\frac{\partial \vec{r}_{22}}{\partial \theta_h} + (\hat{l}_{21} - \hat{l}_{22}).\frac{\partial \vec{r}_{21}}{\partial \theta_h}$$
$$A_{13} = \hat{l}_{32}.\frac{\partial \vec{r}_{32}}{\partial \theta_h} + (\hat{l}_{31} - \hat{l}_{32}).\frac{\partial \vec{r}_{31}}{\partial \theta_h}$$

Here, $\mathbf{A}_{(n\times m)}$, referred to as the structure matrix, represents the linear mapping between the cable tension values, $T_{(m\times 1)}$, and applied torques, $\tau_{(n\times 1)}$. The mapping $\mathbf{A}$ is a function of system geometry and captures the effect of cable routing architecture, cable attachment locations, and actuator positions. For the CDLE cable routing architecture shown in Fig. 1(a), the mapping $\mathbf{A}$ can be represented as in Eq. 2. The vector notations presented in Eq. 2 can be inferred from Fig. 1(b), and the detailed derivation for the mapping can be found in [19]. Essentially, any changes in the cable routing architecture imply changes in the vectors, $\vec{r}$ and $\vec{l}$, in Eq. 2, and subsequent alterations in mapping $\mathbf{A}$.

C. CDLE Intervention

In this study, the CDLE is used to apply a force perturbation to the right leg during the swing phase of the gait cycle aiming to increase the step height, *h*, Fig. 1(b). To achieve it, the CDLE is programmed to apply an upward pull at the ankle equivalent to 10% of the participant's body weight (BW) during the swing phase. It implies, CDLE has to apply an external joint torque across the hip and knee joints through appropriate tension distribution across the cables during the swing phase. Considering the sagittal plane lower-limb as a 2 DOF two-link serial manipulator, the joint torques, τ_{hip} and τ_{knee}, needed to generate the desired upward pull at the ankle can be calculated using the jacobian mapping presented as in Eq. 3 [23]. Here, l_f and l_h represent the length of the femur and tibia. Further, θ_h and θ_k represent the sagittal plane hip and knee joint angles. Subsequently, a quadratic programming problem that solves for the cable tension distribution, *T*, to achieve the desired joint torques, τ_{des}, is presented in Eq. 4. T_{min} and T_{max} denote the lower and upper limits on the cable tension values and were considered as 15 N and 100 N.

$$\begin{bmatrix}\tau_{hip}\\ \tau_{knee}\end{bmatrix} = \begin{bmatrix}-l_f sin(\theta_h) - l_s sin(\theta_h + \theta_k) & -l_s sin(\theta_h + \theta_k)\\ l_f cos(\theta_h) + l_s cos(\theta_h + \theta_k) & l_s cos(\theta_h + \theta_k)\end{bmatrix}\begin{bmatrix}F_x\\ F_y\end{bmatrix} \tag{3}$$

$$\begin{aligned} min: \quad & f(T) = \frac{1}{2}(T - T_P)^T(T - T_P)\\ s.t: \quad & AT = \tau_{des} \quad \text{and} \quad T_{min} \le T \le T_{max}\end{aligned} \tag{4}$$

D. CDLE Control Architecture

Due to the inherent variability in human gait, the gait cycle duration varies from one cycle to another. Subsequently, human continuously adjusts the lower limb movements to accommodate these changes. Thus, to apply the desired force intervention, CDLE must adapt to the changes in walking frequency and detect gait events. Thus, a closed-loop control methodology is considered for the CDLE. Further, it is divided into a high-level controller and a low-level controller to allow for the subject-specific gait adaptation, Fig. 2. This closed-loop

IEEE Robotics and Automation Letters (RA-L) paper, presented at ICRA 2024, Yokohama, Japan. Cite as RA-L paper.

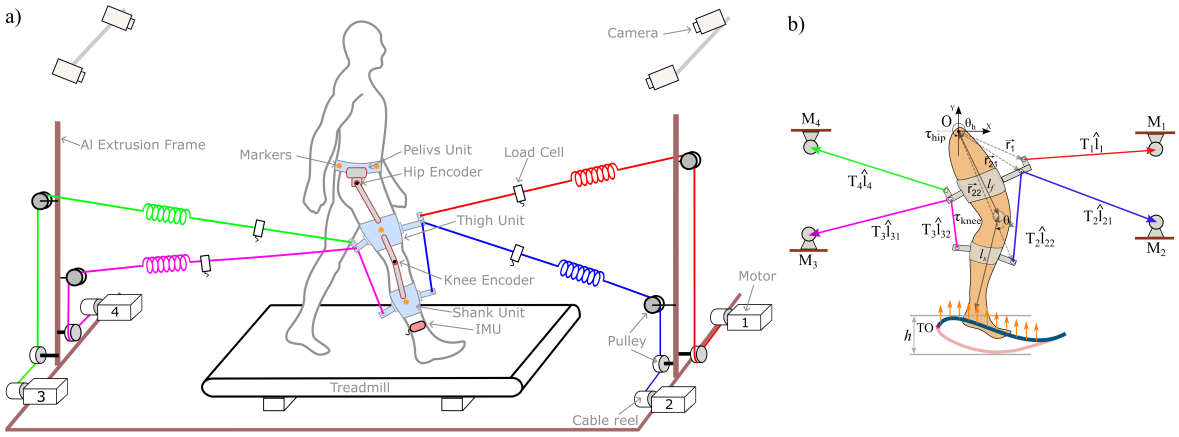

Fig. 1. (a) Schematic of the Cable-Driven Leg Exoskeleton (CDLE) setup highlighting all the components and attachments. Four motors are mounted on a rigid frame, and cables are routed to the subject's lower limb thigh and shank segments using pulleys. Load cells measure the cable tensions, and a spring is placed in series between the motor and load cell. Encoders are used to measure hip and knee joint motions. An eight-camera motion capture system is used to track human motion. (b) Schematic depicting the swing phase intervention using CDLE. Upon detection of the Toe Off (TO) event, the CDLE high-level control generates the desired cable tension profile to increase the step height, *h*.

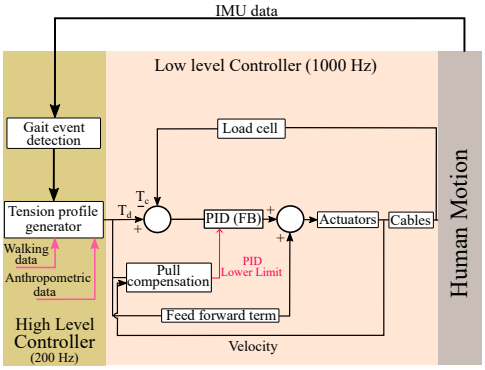

Fig. 2. The control architecture of the CDLE is divided into two parts. The high-level controller tracks the human gait phase and creates the desired tension profile, T_d, necessary to apply desired intervention. The low-level controller implements the T_d values using a constant gain feedforward and PID based feedback terms. A wire pull compensation is added to resolve the cable slackening problem and improve the controller performance.

control runs on SbRIO - 9627, Real-Time (RT) target (National Instruments Inc.), and communication between EPOS 4 (motor controller) and sbRIO RT target is established on CANopen protocol via NI-9881 Module.

High-Level Control: The main goal of the high-level controller is to detect the gait phase during the experiment and then generate the desired cable-tension profile, T_d. It operates at a frequency of 200 Hz. The CDLE uses feedback from an IMU unit attached to the shank to detect the swing and stance phase of gait based on the heel-strike and toe-off events through the gyroscope data of the IMU using a method similar to the one reported in [20]. During the swing phase, the desired cable tensions, T_d, are generated per the desired intervention Eq. 4. Further, in the stance phase, the T_d are commanded to be at 15N to ensure that all the cables are in pretension for the upcoming swing phase.

Low-Level Control: The low-level controller implements the desired cable tension, T_d, at 1000 Hz. A force mode control scheme is used to follow the desired tension values. An open loop reference feed-forward (FF) term with a constant gain for each motor-cable unit and a closed loop PID on the cable tension feedback (FB) term are used, as shown in Fig. 2. The total output defines the motors' input signal (desired current) to actuate the cables in CDLE to achieve the desired tension and to apply the external forces on the lower limb. Since each cable in a cable-driven system can only be operated in tension, the controller needs to avoid issues of cable slackening as it can lead to the cable coming off the pulleys. Accordingly, a pull compensation term is implemented to adaptatively vary the output of the PID for each motor as a function of the motor velocity, *v(t)*, and desired cable tension, T_d, using the method described in [21].

E. Imposed Dynamics Modelling

The dynamics imposed by a robot on the human musculoskeletal system can be modelled as a combination of the robot's inertia, damping, and stiffness elements. In the context of CDLE, considering that only flexible cables are attached to the lower limb, and the device operation happens at normal walking (low speed) conditions, the effects of inertial and damping components on the dynamics are minimal. Thus, the current work predominantly models the CDLE's dynamics through its stiffness characteristics. For a CDLE, external torques are applied at the joints to allow joint motion. Thus, for a quasi-static condition, a slight variation in the joint motion can be related to the joint torque by the joint stiffness as in Eq. 5.

$$\begin{bmatrix} d\tau_{hip} \\ d\tau_{knee} \end{bmatrix} = \begin{bmatrix} K_{HH} & K_{HK} \\ K_{KH} & K_{KK} \end{bmatrix} \begin{bmatrix} d\theta_h \\ d\theta_k \end{bmatrix}$$
$$d\tau = \mathbf{K}_\theta d\theta \tag{5}$$

Here, $\mathbf{K}_\theta$ is the multi-joint stiffness matrix which denotes the relation between joint torques and angles. Elements K_{HH} and K_{HK} represent stiffness at the hip joint, and elements K_{KH} and K_{KK} represent stiffness at the knee joint. The incremental cable displacement, dl, and the incremental tension in cables, dT, are related by the diagonal cable stiffness

IEEE Robotics and Automation Letters (RA-L) paper, presented at ICRA 2024, Yokohama, Japan. Cite as RA-L paper.

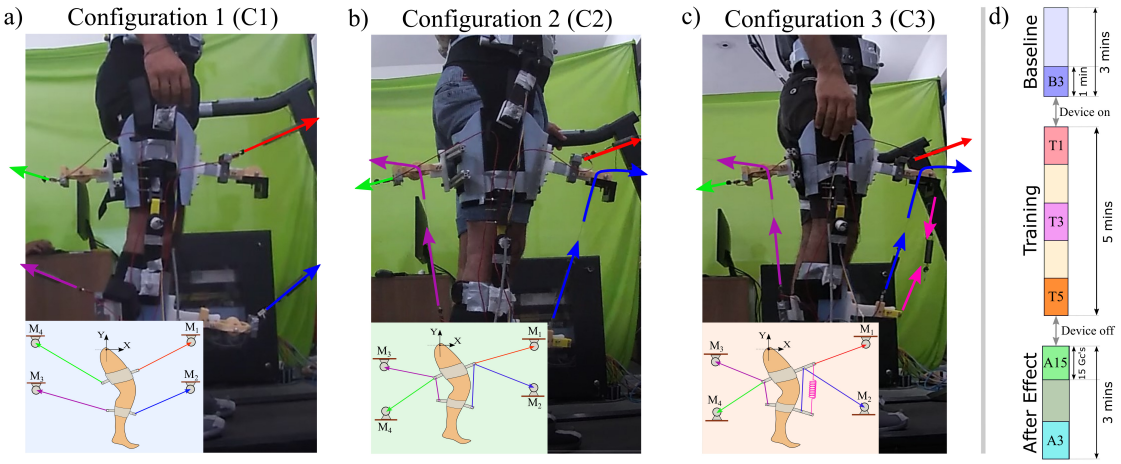

Fig. 3. Three different CDLE cable routing configurations. (a) Configuration 1 (***C1***): All four cables are connected directly to the thigh and shank segments. (b) Configuration 2 (***C2***): Two cables are routed through the thigh to connect to the anterior and posterior parts of the shank. The remaining two cables are connected directly to the thigh. (c) Configuration 3 (***C3***) : Cable routing remains similar to C2, but an additional spring element is connected between the thigh and shank segments. (d) Experimental protocol for the human experiment included baseline, training, and after effect sessions.

matrix, k_c as $dT = k_c dl$. Now, differentiating Eq. 1 and substituting $d\tau$, dT, and $dl = -\mathbf{A}^T d\theta$ in the obtained equation results in the expression for $\mathbf{K}_\theta$ as in Eq. 6 [19]. Essentially, any alterations in the cable routing architecture of CDLE imply changes in $\mathbf{A}$, which subsequently alters the multi-joint stiffness, $\mathbf{K}_\theta$, characteristics, i.e., transforming the nature of imposed stiffness at anatomical hip and knee joints by CDLE.

$$\mathbf{K}_\theta = \left[\frac{d\mathbf{A}}{d\theta_h}T \quad \frac{d\mathbf{A}}{d\theta_k}T\right] - \mathbf{A}k_c\mathbf{A}^T \tag{6}$$

III. CDLE Experiment

To elaborate on the role of the imposed dynamics, we studied human locomotor adaptation for the same external force intervention using three different CDLE cable routing configurations. Essentially, the objective of the intervention, which is to increase the step height during the swing phase, can be achieved by increasing hip joint flexion, knee joint flexion or by the combination of both joints. Thus, the choice of the configurations is specifically due to the nature of the distinct dynamics they impose at the human anatomical joints (explained in detail in Section III-B) to facilitate the invocation of a particular joint strategy. Figure 3 presents a representative picture showing participants donned with three CDLE configurations.

In Configuration 1, ***C1***, the four cables of the CDLE are directly connected to the anterior and posterior sides of the thigh and shank units to administer the external forces, Fig. 3(a). In Configuration 2, ***C2***, the cables connecting the anterior and posterior sides of the shank unit are routed through the thigh unit, and the remaining two cables are connected directly to the thigh unit as shown in Fig. 3(b). Further, in Configuration 3, ***C3***, the cable routing remains similar to ***C2***. However, an additional passive spring is connected between the anterior side of the thigh and shank units as shown in Fig. 3(c).

A. Experimental Protocol

Twenty-four healthy males in the age range 19–27 years (mean age: 23.5 years) and mean weight 71.25 kg (SD: 7.5 kg), participated in the experiment where eight subjects were tested for each of the three CDLE configurations. Subjects were informed about the experimental procedure and signed a written consent form approved by the Institute Ethics Committee of the Indian Institute of Technology Gandhinagar (Identifier number: IEC/VV/2021/013) before participation. The experiment involved three sessions in the order of Baseline (B), Training (T), and After effect (A), refer Fig. 3(d). In all three sessions, each participant walked on a treadmill at a constant speed of 3 kmph. The experiment began with the B session, which lasted for 3 minutes. A break of 5 min was given before starting the training, T, session to engage the CDLE and to compute the desired force profile. The T session lasted 5 minutes, where the CDLE applied the swing phase force intervention on the participants' right leg. Following the T session, the cables were removed immediately. The participant walked for another three minutes at the same treadmill speed of 3 kmph as part of the After effect, A, session. Sixteen reflective markers were attached to anatomical key points on the lower limb according to the plug-in gait template in the Motion Capture System's Nexus software for acquiring gait parameters. Data were recorded for all the sessions.

B. Imposed Stiffness

Figure 4(a-c) presents the average hip, knee, and coupling stiffness imposed on human anatomical joints by the three CDLE configurations. The data shown are the representative data computed from one representative subject from each group of the CDLE experimental session. The human lower limb joint kinematics data, θ_h and θ_k, cable tension data, T, cable stiffness values, k_c, and cable attachment parameters were used to compute $\mathbf{K}_\theta$ using Eq. 5. Notably, the characteristics of the imposed stiffness are distinct for the three CDLE configurations. These differences are governed by the changes in the structure matrix, A, in Eq. 5 across the CDLE configurations as presented in [19], [22]. For the current study, Eq. 2 presents the mapping $\mathbf{A}$ for the CDLE configuration ***C2***. While for ***C1***, the second and third columns of $\mathbf{A}$ in Eq.

IEEE Robotics and Automation Letters (RA-L) paper, presented at ICRA 2024, Yokohama, Japan. Cite as RA-L paper.

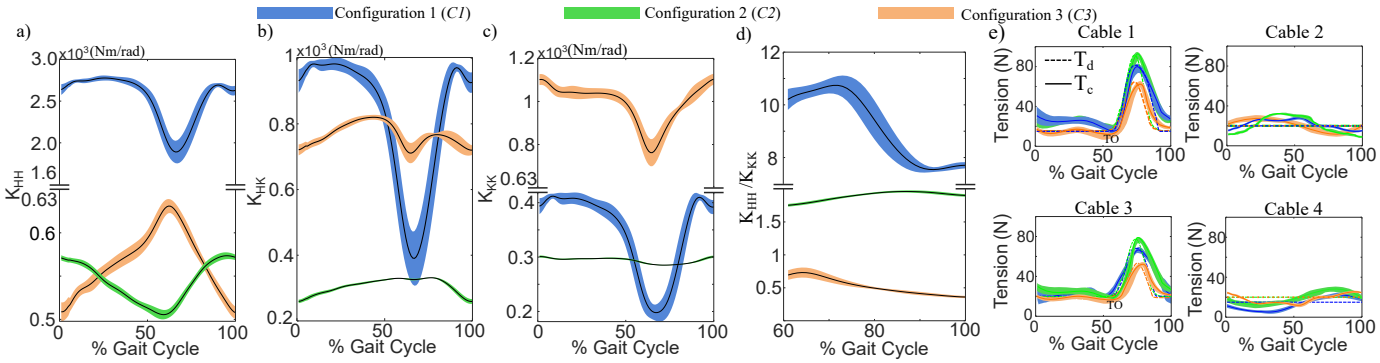

Fig. 4. (a)-(c) A representative plot of the imposed joint stiffness (N-m/rad) at lower limb human anatomical joints by the three CDLE configurations. The solid line represents the stiffness imposed by CDLE during the training session over one minute. The shaded area region represents the standard deviation. (d) Ratio of imposed stiffness at hip and knee joints. (e) A representative plot showcasing the cable tension distribution of the three CDLE configurations across the gait cycle to apply the required force intervention. The dotted line represents the desired cable tension, T_d, and the solid line represents the averaged cable tension, T_c, applied by CDLE during the session over one minute. The shaded area region represents the standard deviation of the T_c.

2 change to reflect the routing difference of cables 2 and 3. Similarly, for ***C3***, a term corresponding to the passive spring gets added to **A** in Eq. 2. From Fig. 4(a), it is observed that configuration ***C1*** imposed a large stiffness at hip joint, K_{HH}, than ***C2*** and ***C3***. Imposed coupling stiffness is more dominant in ***C1*** and ***C3***, than in ***C2***, Fig. 4(b). Further, the imposed stiffness at the knee joint, K_{KK}, is very high for ***C3*** and nearly constant throughout the gait cycle for ***C2***, refer Fig. 4(c). For ***C1***, K_{KK} varies significantly across the gait cycle.

Configuration 1 (C1): For ***C1***, it is observed that the stiffness imposed by CDLE at the hip joint, K_{HH}, is larger than the knee, K_{KK}, throughout the gait cycle, Figs. 4(a) and (c). Figure 4(d) presents the ratio $\frac{K_{HH}}{K_{KK}}$, during the swing phase. It is observed that imposed stiffness at the hip joint is at least eight times larger than the knee during this phase. Notably, ***C1*** imposes a stiffness of magnitude between (1800 - 2600)N-m/rad at the hip joint and between (200 - 400)N-m/rad at the knee joint. *For the case of an external force intervention during the swing phase, considering that **C1** imposes dominant stiffness at the hip joint, it is hypothesized that subjects will prefer a distal joint strategy, i.e., using their knee joint to adapt to the intervention.*

Configuration 2 (C2): For ***C2***, similar to ***C1***, the stiffness imposed by CDLE at the hip joint, K_{HH}, is larger than knee, K_{KK}, throughout gait cycle, Figs. 4(a) and (c). However, it is to be noted that the magnitude of this imposed stiffness is significantly smaller for ***C2*** than ***C1***. In particular, the imposed stiffness magnitude is between (500 - 600)N-m/rad at the hip joint and (280 - 300)N-m/rad at the knee joint. Further, for ***C2***, the ratio $\frac{K_{HH}}{K_{KK}}$ is smaller during swing phase than ***C1***, Fig. 4(d). Notably, this variation is comparable to the musculoskeletal hip and knee joint stiffness ratio during swing phase presented in [24]. *For the case of an external force intervention during the swing phase, considering that **C2** imposes the stiffness characteristics similar to the musculoskeletal stiffness at anatomical joints, we hypothesize that subjects will effectively use the combination of hip and knee joints to adapt to the intervention.*

Configuration 3 (C3): For ***C3***, the stiffness imposed by CDLE at knee, K_{KK}, is dominant than hip, K_{HH}, throughout the gait cycle, Figs. 4(a) and (c). The magnitude of this imposed stiffness at the hip joint is between (500 - 620)N-m/rad. For ***C3***, unlike ***C1*** and ***C2***, the ratio $\frac{K_{HH}}{K_{KK}}$ is smaller than unity during swing phase, implying dominant knee stiffness, Fig. 4(d). Notably, the cable-routing in ***C3*** remained similar to ***C2***, but addition of the passive spring in ***C3*** facilitated imposition of additional stiffness at knee joint without affecting hip stiffness. Further, it can also be observed that this ratio decreases as the swing phase progresses. *For the case of an external force intervention during the swing phase, considering that **C3** imposes dominant stiffness at the knee joint, we hypothesize that subjects will prefer a proximal joint strategy, i.e., using their hip joint to adapt to the intervention.*

C. Data Analysis

For data analysis, we used data from the third minute of the B session, referred to as B3. The T session's first, third, and fifth-minute data are considered, referred to as T1, T2, and T3, respectively. Further, two data sets of the A session, A15: first 15 gait cycles data, and A3: third minute data, are considered. Gait parameters, namely step height, h, peak hip joint flexion, and peak knee joint flexion were computed for each gait cycle for the three CDLE configurations. Averaged data of these parameters during B3, T1, T2, T3, A15, and A3 were analyzed statistically for each CDLE configuration. Shapiro Wilk test and Lilliefors test were used to test the normality condition. A one-way analysis of variance with repeated measures of a CDLE configuration was performed on these parameters. A pairwise comparison among the sessions was conducted using the Bonferroni test for the post hoc analysis. All statistical analyses were performed using OriginPro software, and p-values of < 0.05 were considered statistically significant.

IV. Results

The intervention during the swing phase in the training session resulted in noticeable changes in the participant's hip and knee joint kinematics when compared with their baseline for all three CDLE configurations, Figs. 5, 6 and 7. Also, noticeable changes were observed in the step height, h, of the perturbed leg during the training session, implying that the

IEEE Robotics and Automation Letters (RA-L) paper, presented at ICRA 2024, Yokohama, Japan. Cite as RA-L paper.

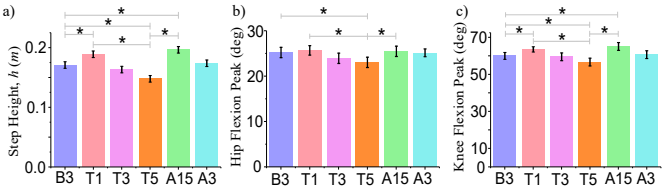

Fig. 5. (a) Step height (h) variations of the perturbed leg for different sessions for Configuration 1 (***C1***). (b) and (c) Mean peak flexion of hip and knee joints of the perturbed leg for different sessions during the swing phase. The data presented here are averaged across all the participants of ***C1***. with standard error. Asterisks show the significant pairs from post-hoc test ($*p < 0.05$).

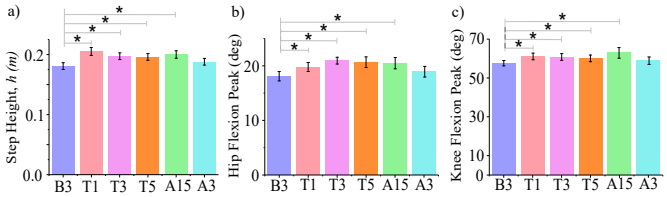

Fig. 6. (a) Step height (h) variations of the perturbed leg for different sessions for Configuration 2 (***C2***). (b) and (c) Mean peak flexion of hip and knee joints of the perturbed leg for different sessions during the swing phase. The data presented here are averaged across all participants of ***C2*** with standard error. Asterisks show the significant pairs from post-hoc test ($*p < 0.05$).

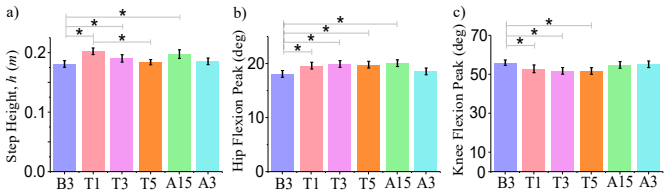

Fig. 7. (a) Step height (h) variations of the perturbed leg for different sessions for Configuration 3 (***C3***). (b) and (c) Mean peak flexion of hip and knee joints of the perturbed leg for different sessions during the swing phase. The data presented here are averaged across all participants of ***C3*** with standard error. Asterisks show the significant pairs from post-hoc test ($*p < 0.05$).

adopted hardware and control strategy was adequate to apply the intended force intervention.

Figure 4(e) presents a representative plot of the tension profile of all the cables across the gait cycle during the training session of the three CDLE configurations. The shaded region along the curve highlights the standard variation of the cable tension over one minute. The intended force perturbation tends to increase the step height, h, during the swing phase of walking, implying the application of external joint torque by CDLE to extend the hip and knee flexion. Cables 1 and 3, which connect to the anterior side of the thigh unit and the posterior side of the shank unit, respectively, are mainly involved, refer to Fig. 3. The other two cables, 2 and 4, maintain a constant tension value to avoid cable slackening. As the desired force at the ankle is a function of the subject's body weight, the cable tension profile varies from subject to subject and between cable routing configurations.

Configuration 1 (C1)*:* Figure 5(a) compares the variation of the step height, h, across the experimental sessions. The statistical analysis reported significant differences between sessions in h. The post-hoc pairwise analysis reported that h increased significantly during the first minute of the training session, T1, compared to the baseline, B (B3-T1: p = 0.046). However, no significant difference is observed between B3-T3, implying h coming back to the baseline value. Interestingly, h reduced further as the training progressed, T5, which is significant compared to B3, (B3-T5: p = 0.013). Also, a significant difference is observed between T1-T5 (p = 0.009), implying the variations in h during the training session. Further, with higher h value during A15, significant after-effects are observed between B3-A15 (p =0.039) and T5-A15 (p =0.0012). However, h restored to the baseline value as the A session progressed, as no significant difference was observed between B3-A3.

Figure 5(b) shows the variation of the mean peak hip joint flexion during the swing phase of the perturbed leg across the experimental sessions. Hip joint flexion is larger initially in the training session, T1, though not statistically significant, but its values reduced as the training session progressed to result in a significant difference between B3-T5 (p = 0.036), T1-T5 (p = 0.041), and T5-A15 (p = 0.0021). Further, no significant after-effects are observed at the hip joint compared with B. Figure 5(c) shows the mean peak knee joint flexion variation during the swing phase of the perturbed leg across the experimental sessions. The knee joint flexion increased initially in the training session and reduced as the session progressed. The increase in knee flexion peak during T1 is significant compared to B3 (B3-T1: p = 0.041). This implies participants flexed the knee joint more in response to the perturbation during T1. The knee flexion reduced as the training progressed such that the reduction is significant between B3-T5 (p = 0.04) and T1-T5 (p = 0.02). Further, a significant difference is observed between B3-A15 (p = 0.034), where higher knee flexion is observed during A15 implying after-effects.

Configuration 2 (C2)*:* Figure 6(a) compares the variation of the step height, h, across the experimental sessions. The statistical analysis reported differences in step height, h, of the perturbed leg between the sessions. The post-hoc pairwise analysis reported an increase in h during the training session compared to the baseline (B3-T1: p = 0.036, B3-T3: p = 0.041, B3-T5: p = 0.042). However, no significant differences are observed between the data sets of the training session, i.e., T1, T3, and T5, implying that the increase in h is retained throughout the T session. Furthermore, a significant difference is observed between B3-A15 (p = 0.03) with higher h for A15, implying after-effects.

Figure 6(b) compares the variation of the perturbed leg's mean peak hip joint flexion across the experimental sessions. A significant increase in hip joint flexion is observed during the training session compared with baseline (B3-T1: p = 0.045, B3-T3: p = 0.028, B3-T5: p = 0.022). This increase is retained throughout the training session (T1-T3, T3-T5, T1-T5 not significant). Also, a significant after-effect with higher hip flexion in A15 is observed, B3-A15 (p=0.031). Further, Fig. 6(c) compares the perturbed leg's mean peak knee joint flexion across the experimental sessions. A significant increase is reported in the knee joint flexion during the training session compared with baseline (B3-T1: p = 0.045, B3-T3: p = 0.041, B3-T5: p = 0.04). Notably, this increase is retained during

IEEE Robotics and Automation Letters (RA-L) paper, presented at ICRA 2024, Yokohama, Japan. Cite as RA-L paper.

the training session (T1-T3, T3-T5, T1-T5 not significant). Further, a significant after-effect with higher knee flexion in A15 is observed, B3-A15 (p=0.023).

Configuration 3 (C3): The statistical analysis reported differences in the values of the step height, h, of the perturbed leg between the sessions, Fig. 7(a). The pairwise post-hoc analysis reported significance between B3-T1 (p = 0.0205) and B3-T3 (p = 0.041), but no significance between B3-T5. This implies that the step height increased during the initial phase of the training session and returned to the baseline as the training session progressed. A significant reduction is observed during the training, T1-T5 (p = 0.02). A significant after-effect is observed with larger h in A15 (B3-A15: p = 0.03).

Figure 7(b) compares the variation of the perturbed leg's mean peak hip joint flexion across the experimental sessions. A significant increase in hip joint flexion is observed during the training session compared with baseline (B3-T1: p = 0.0423, B3-T3: p = 0.024, B3-T5: p = 0.026). This increase is retained throughout the training session (T1-T3, T3-T5, T1-T5 not significant). Significant after-effect with higher hip flexion in A15 is observed, B3-A15 (p=0.019). Further, Fig. 7(c) compares the mean peak knee flexion across the experimental sessions. A significant reduction in knee joint flexion is observed throughout the training session compared with baseline (B3-T1: p = 0.0416, B3-T3: p = 0.0391, B3-T5: p = 0.0403). This reduction is retained throughout the training session (T1-T3, T3-T5, T1-T5 not significant). Further, no significant difference is observed between B3-A15, implying no after-effect at the knee joint.

V. Discussion

In a robotic intervention paradigm, the use of a robotic exoskeleton is aimed at either assisting or resisting the human lower limb joint motion to emulate a desired gait as per the intended intervention [25]–[27]. In general, a task space approach is taken, where the joint torque values required for a multi-link serial-chain model of a leg to execute a desired trajectory in the task space are administered. To apply the computed torque values on the human leg, external forces are applied by the robotic system at the leg segments, such as the thigh and shank. Notably, human lower limbs have redundant DOFs and are redundantly actuated through muscles, i.e., redundant musculoskeletal system. Essentially, from a human perspective, there exist multiple ways of actuating muscles to achieve a particular task space performance. Thus, there can be cases where the musculoskeletal system adjusts differently than the intended aim of the applied intervention during a physical human-robot interaction (pHRI) task. This makes it critical to comprehend the aspect of pHRI in a robotic intervention paradigm. Notably, several works [28]–[31], have discussed the importance of the pHRI in promoting the desired outcome of the intervention. In this context, the current study has provided insights into how the external dynamics of a robot can drive a subject to choose a particular joint strategy in response to a specific gait intervention.

Three different CDLE architectures, which impose contrasting external stiffness at anatomical joints but are programmed to execute a similar intervention, are considered for this study. The variation in the imposed stiffness is achieved by altering the cable routing configurations along the human lower limb, thigh, and shank segments. Specifically, we observed diverse lower limb joint kinematic responses from the experimental results by the three subject groups for the same gait intervention. For the case of CDLE Configuration 1, ***C1***, which imposes large stiffness at the hip than the knee joint, it is observed that the subjects adopted the distal joint strategy, as hypothesized. Specifically, subjects flexed their knee more when the applied forces to increase the step height were applied. Further, the desired goal of the intervention, i.e., to increase step height, h, during the swing phase was not entirely achieved during the training session. As ***C1*** imposed a large magnitude of stiffness at the anatomical joints, reduced step height due to reduced joints' range of motion was observed as the training progressed. This elaborates the importance of pHRI in an intervention, as in this case, CDLE is administering forces to increase h, but the resulting outcome is against the intended intervention.

The results from the healthy human experiments with CDLE Configuration 2, ***C2***, showed that subjects preferred using both the hip and knee joints, i.e., the combination of both joints, in response to force intervention, as hypothesized. Further, the step height, h, increased during the training session and was maintained throughout the session, implying the fulfillment of the desired intervention. Since the gait intervention was the same for both ***C1*** and ***C2***, the reason for the different gait adaptation is due to the significant difference between the imposed joint stiffness by ***C1*** and ***C2***. Especially, unlike ***C1***, the range and trend of the ***C2*** imposed stiffness was comparable with the lower-limb musculoskeletal stiffness [24]. For the CDLE Configuration 3, ***C3***, the subjects adopted an entirely different musculoskeletal response. As ***C3*** imposed a significantly large stiffness at the knee joint than the hip, it is observed that the subjects adopted the proximal joint strategy as hypothesized. Specifically, subjects flexed their hip more when the applied forces to increase the step height were applied. Similar to the case of ***C1***, the desired goal of the intervention, i.e., to increase step height, h, was not entirely achieved during the training session of ***C3***.

Overall, all three groups showed varied gait responses such that the subjects used either predominantly their hip joint, knee joint, or a combination of both joints for the same intervention. The step height changes in the present study are in agreement with the observations presented in [15], [16] but differed from [14]. Notably, gait adaptation due to imposed joint stiffness has been of interest in the literature [31]–[33]. Specifically, gait adaptation due to changes in stiffness at the hip joint over a gait cycle has been reported using a rigid hip exoskeleton in [31], [32]. The effects of stiffness and damping on the ankle joint have been studied in [33], [34]. For the case of a therapeutic intervention, a trained therapist uses both his/her upper limbs and skillfully alters his/her upper-limb joint stiffness, i.e., imposed dynamics, to generate the desired lower-limb motion in the subject. On similar lines, in the presented study, we altered the imposed stiffness by exoskeleton at a particular joint and invoked a specific joint strategy in the subject.

This study showcased the importance of external dynamics

in a robotic intervention in invoking different musculoskeletal responses. The observed results demonstrated the CDLE's ability to alter pHRI to promote a particular joint strategy and also highlighted the importance of the choice of cable routing in a CDLE based intervention. The results derived from this study also identify stiffness as an adequate parameter to model the imposed dynamics and also were able to map it to the outcome of the robotic intervention. Essentially, the analysis of gait changes in robot-aided walking, when compared to free natural walking, as addressed in the present study, is expected to clarify and elaborate upon key aspects of pHRI that serve as a building block for future robot designs or optimized use of existing devices by incorporating imposed dynamics understanding to promote subject-specific interventions. Further, the presented results bear significance as the exoskeletons are used for individuals with disabled walking, and any unaccounted dynamics can lead to undesired compensatory strategies by the individuals.

One of the limitations of the current study is smaller number of participants. Further experiments with a diverse population group are required to generalize the presented observations. Notably, the current results serve as a basis for designing such studies. Such understanding can eventually help in designing subject-specific rehabilitation paradigms. However, as the current paradigm was tested on healthy individuals, further research is needed to ascertain how to alter imposed dynamics to benefit elderly and neurologically affected populations. Considering adaptation during walking, a study targeting step-length perturbations will be of interest as literature [14] report gait adaptation when step-length is altered. Even though the current work reported successful implementation of cable tension by the CDLE, the controller can be further improved for proper pre-tensioning and tracking.

ACKNOWLEDGMENT

This work was conducted with the facility built, which was supported by the corresponding Author's Institute and sponsored research grants.

REFERENCES

[1] Patterson, Kara K., et al. "Evaluation of gait symmetry after stroke: a comparison of current methods and recommendations for standardization." Gait and posture 31.2 (2010): 241-246.

[2] Baker, Jessica M. "Gait disorders." The American journal of medicine 131.6 (2018): 602-607.

[3] Burnfield, M. "Gait analysis: normal and pathological function." Journal of Sports Science and Medicine 9.2 (2010): 353.

[4] Gordon, Keith E., and Daniel P. Ferris. "Learning to walk with a robotic ankle exoskeleton." Journal of biomechanics 40.12 (2007): 2636-2644.

[5] Fritz, Heather, et al. "Robotic exoskeletons for reengaging in everyday activities: promises, pitfalls, and opportunities." Disability and rehabilitation 41.5 (2019): 560-563.

[6] Rodríguez-Fernández, et al. "Systematic review on wearable lower-limb exoskeletons for gait training in neuromuscular impairments." Journal of neuroengineering and rehabilitation 18.1 (2021): 1-21.

[7] Yan, Tingfang, et al. "Review of assistive strategies in powered lower-limb orthoses and exoskeletons." Robotics and Autonomous Systems 64 (2015): 120-136.

[8] Chen, Bing, et al. "Recent developments and challenges of lower extremity exoskeletons." Journal of Orthopaedic Translation 5 (2016): 26-37.

[9] Sanjeevi, N. S. S., Yogesh Singh, and Vineet Vashista. "Recent advances in lower-extremity exoskeletons in promoting performance restoration." Current Opinion in Biomedical Engineering 20 (2021): 100338.

[10] Van Hedel, Hubertus JA, et al. "Advanced Robotic Therapy Integrated Centers (ARTIC): an international collaboration facilitating the application of rehabilitation technologies." Journal of neuroengineering and rehabilitation 15 (2018): 1-16.

[11] Colombo, Gery, et al. "Treadmill training of paraplegic patients using a robotic orthosis." Journal of rehabilitation research and development 37.6 (2000): 693-700.

[12] Ahn, Jooeun, and Neville Hogan. "Walking is not like reaching: evidence from periodic mechanical perturbations." PloS one 7.3 (2012): e31767.

[13] Hidler, Joseph, et al. "Multicenter randomized clinical trial evaluating the effectiveness of the Lokomat in subacute stroke." Neurorehabilitation and neural repair 23.1 (2009): 5-13.

[14] Cajigas, Iahn, et al. "Robot-induced perturbations of human walking reveal a selective generation of motor adaptation." Science Robotics 2.6 (2017): eaam7749.

[15] van Asseldonk, Edwin HF, Bram Koopman, and Herman van der Kooij. "Locomotor adaptation and retention to gradual and sudden dynamic perturbations." 2011 IEEE International Conference on Rehabilitation Robotics. IEEE, 2011.

[16] Emken, Jeremy L., and David J. Reinkensmeyer. "Robot-enhanced motor learning: accelerating internal model formation during locomotion by transient dynamic amplification." IEEE Transactions on Neural Systems and Rehabilitation Engineering 13.1 (2005): 33-39.

[17] Xiong, Hao, and Xiumin Diao. "A review of cable-driven rehabilitation devices." Disability and Rehabilitation: Assistive Technology 15.8 (2020): 885-897.

[18] Rezazadeh, Siavash, and Saeed Behzadipour. "Workspace analysis of multibody cable-driven mechanisms." (2011): 021005.

[19] Sanjeevi, N., and Vashista, V. (2021). Stiffness modulation of a cable-driven leg exoskeleton for effective human–robot interaction. Robotica, 39(12), 2172-2192. doi:10.1017/S0263574721000242

[20] Singh, Yogesh, and Vineet Vashista. "Gait Classification With Gait Inherent Attribute Identification From Ankle's Kinematics." IEEE Transactions on Neural Systems and Rehabilitation Engineering 30 (2022): 833-842.

[21] Vashista, Vineet. A cable-driven pelvic robot: Human gait adaptation and rehabilitation studies. Columbia University, 2015.

[22] Sanjeevi, N. S. S., and Vineet Vashista. "Effect of passive springs on taskspace stiffness of a cable-driven serial chain manipulator." Recent Advances in Machines and Mechanisms: Select Proceedings of the iNaCoMM 2021. Singapore: Springer Nature Singapore, 2022. 601-612.

[23] Lynch, Kevin M., and Frank C. Park. Modern robotics. Cambridge University Press, 2017.

[24] Stanev, Dimitar, and Konstantinos Moustakas. "Stiffness modulation of redundant musculoskeletal systems." Journal of biomechanics 85 (2019): 101-107.

[25] Anam, Khairul, and Adel Ali Al-Jumaily. "Active exoskeleton control systems: State of the art." Procedia Engineering 41 (2012): 988-994.

[26] Hidayah, Rand, et al. "Comparing the performance of a cable-driven active leg exoskeleton (C-ALEX) over-ground and on a treadmill." 2018 7th IEEE International Conference on Biomedical Robotics and Biomechatronics (Biorob). IEEE, 2018.

[27] Hobbs, Bradley, and Panagiotis Artemiadis. "A review of robot-assisted lower-limb stroke therapy: unexplored paths and future directions in gait rehabilitation." Frontiers in neurorobotics 14 (2020): 19.

[28] Belda-Lois, Juan-Manuel, et al. "Rehabilitation of gait after stroke: a review towards a top-down approach." Journal of neuroengineering and rehabilitation 8 (2011): 1-20.

[29] Iosa, Marco, et al. "Driving electromechanically assisted Gait Trainer for people with stroke." Journal of Rehabilitation Research and Development 48.2 (2011): 135-146.

[30] Morone, Giovanni, et al. "Who may benefit from robotic-assisted gait training? A randomized clinical trial in patients with subacute stroke." Neurorehabilitation and neural repair 25.7 (2011): 636-644.

[31] Lee, Jongwoo, et al. "Applying hip stiffness with an exoskeleton to compensate gait kinematics." IEEE Transactions on Neural Systems and Rehabilitation Engineering 29 (2021): 2645-2654.

[32] Lee, Jongwoo, et al. "Modulating hip stiffness with a robotic exoskeleton immediately changes gait." 2020 IEEE International Conference on Robotics and Automation (ICRA). IEEE, 2020.

[33] Azocar, et al. "Stiffness perception during active ankle and knee movement." IEEE Transactions on Biomedical Engineering 64.12 (2017): 2949-2956.

[34] C. Jategaonkar, et al, "Effect of External Damping on Ankle Motion During the Swing Phase of Walking," in IEEE Robotics and Automation Letters, vol. 7, no. 3, pp. 7612-7619, July 2022, doi: 10.1109/LRA.2022.3184781.

IEEE Robotics and Automation Letters (RA-L) paper, presented at ICRA 2024, Yokohama, Japan. Cite as RA-L paper.